SLICE: A Semi-Lagrangian Inherently Conserving and Efficient scheme for transport problems*†

MOHAMED ZERROUKAT‡, NIGEL WOOD and ANDREW STANIFORTH

20th December 2002

Abstract

A Semi-Lagrangian Inherently Conserving and Efficient (SLICE) scheme is described for transport of passive scalars in Cartesian geometry. It is based on a Control-Volume (CV) approach and uses multiple sweeps of a 1D $O\left(\Delta x^4\right)$ conservative remapping algorithm along pre-determined cascade directions. The scheme has been applied to standard 2D tests from the literature. Overall, it is found that in addition to exactly conserving mass, it is also competitive with standard non-conserving semi-Lagrangian schemes from the viewpoints of both computational efficiency and accuracy.

1 Introduction

Semi-Lagrangian (SL) advection schemes have become very popular (Temperton, Hortal & Simmons 2001) for meteorological/atmospheric modelling because of the substantial savings that can accrue from lengthening the stability-limited timesteps of traditional Eulerian schemes. For a review of SL schemes and related issues, see Staniforth & Côté (1991). Unlike the Eulerian flux-form approach, a common problem with SL schemes is the lack of conservation of quantities, such as mass, due to interpolation. Although exact conservation may not be crucial for some applications, e.g. Numerical Weather Prediction (NWP) where the integration period is relatively short, it can be of paramount importance for long simulations, e.g. those of climate studies. Even though it is not essential for NWP, if exact conservation can be achieved without major computational overhead, it is nevertheless desirable.

Various authors have tackled this issue and a number of conserving SL schemes have appeared in the literature. Such schemes may be grouped in two categories: (i) corrective, and (ii) inherently-conservative schemes. Algorithms in the first group, e.g. the quasi-conservative algorithm of Priestley (1993), are *a posteriori* corrections to restore the desired quantity whilst minimising changes to the original solution. Attention herein is focussed on the second group.

†Appeared in: Q. J. R. Meterol. Soc. (**2002**), vol. 128, pp. 2801-2820

‡Corresponding author: *Dr M Zerroukat, Met Office, London Road, Bracknell, Berkshire RG12 2SZ, UK. E-mail: mohamed.zerroukat@metoffice.com*

Most inherently-conservative semi-Lagrangian schemes are either relatively computationally expensive with respect to the improvement expected, or not easy to generalise efficiently for 3D global circulation models. The most elegant schemes are for 1D problems (e.g. Laprise & Plante (1995), Rancic (1995)). However, a computationally efficient extension of these mappings to higher dimensions is not an easy task due to the distorted (when viewed in real space) Lagrangian grid. Rancic (1992), hereinafter referred to as R92, presented a natural extension to 2D of a 1D mapping. It employs a bi-parabolic piecewise representation and the gridbox-averaged field is computed by exactly integrating the piecewise representation over a Lagrangian control volume (CV). This entails considerable geometric complexity due to the distorted nature of the Lagrangian CV, an irregular quadrilateral when represented in real space, making the scheme both complex and expensive, and particularly so in 3D. Scroggs & Semazzi (1995) presented a somewhat simpler piecewise-constant version of R92, but with the consequence of being highly damping. To overcome the complexities of R92, Laprise & Plante (1995) advocated tracing back the centre of the Eulerian CV edges, rather than the corners as in R92, and the resulting Lagrangian CV's are then rectangles in real space by construction. This, however, is not a very robust approach as Lagrangian CV's may overlap and exact conservation is then lost. In a series of papers (Machenhauer & Olk (1996), Machenhauer & Olk (1997), Nair & Machenhauer (2002), Nair, Scroggs & Semazzi (2002)), Machenhauer, Nair and collaborators tried to simplify the remapping by approximating the irregular Lagrangian CV by a series of regular sub-CV's. Although this is a reasonable approximation, as long as the Lagrangian grid is relatively smooth, the complexity of the underlying sub-CV topology for general flows leads to algorithmic complexity. Unlike the above CV-based methods which are both locally and globally conserving, Leslie & Purser (1995) developed a simpler, grid-based, scheme which is globally conserving. The scheme exploits some of the features of cascade interpolation developed previously by the same authors (Purser & Leslie 1991) and the use of cumulative mass and density fields which are staggered with respect to each other. The cumulative mass function is computed by integrating the density distribution, whilst density is recovered by differentiating the mass function. By virtue of differentiation over contiguous zones, *global* mass is conserved as in flux-form discretisations. However, as noted in Purser (1998), the scheme does not adequately handle singularities such as polar points in a latitude-longitude grid, and this limitation has hindered its application to global models.

Here an efficient 2D inherently-conservative semi-Lagrangian scheme, that exploits some of the best features of the above-mentioned algorithms, is developed and tested. The 2D version of the scheme (SLICE-2D) combines the accuracy of the 1D $O\left(\Delta x^4\right)$ conservative remapping algorithm (SLICE-1D) with the computational efficiency of solving higher-dimension problems by multiple sweeps of the SLICE-1D algorithm along predefined Eulerian-Lagrangian cascade directions. At each sweep this means that only CV's of constant width (on the appropriate mesh) arise, thereby allowing the inherent efficiency of the 1D algorithm to be fully exploited. The first stage is performed in the regular Eulerian (Cartesian) frame, while the second is entirely computed in the (regular) Lagrangian frame. This is similar to the algorithm of Nair et al. (2002), but without the complexity of explicitly computing the area (or volume) of complex Lagrangian CV's in physical space.

The rest of the paper is organised as follows: Section 2 illustrates the details of the SLICE-1D scheme,

while SLICE-2D is detailed in Section 3. Results of several tests from the literature are given in Section 4, and conclusions are summarised in Section 5.

2 The SLICE-1D scheme

Consider passive 1D advective transport of a scalar quantity ρ governed, in the absence of sources and sinks, by

$$\frac{\partial \rho}{\partial t} + \frac{\partial}{\partial x}(u\rho) = 0, \tag{2.1}$$

where $\rho(x,t)$ is the density (amount of scalar per unit length) of the transported quantity, and $u(x,t)$ is the transporting velocity field.

Integrating (2.1) with respect to x between two arbitrary moving boundaries $x_1 = x_1(x,t)$ and $x_2 = x_2(x,t)$, and making use of Leibniz' rule, leads to (Laprise & Plante 1995)

$$\begin{aligned} \frac{d}{dt}\int_{x_1(x,t)}^{x_2(x,t)} \rho dx - \left[\rho\left(x_2,t\right)\frac{dx_2}{dt} - \rho\left(x_1,t\right)\frac{dx_1}{dt}\right] \\ + \left[\rho\left(x_2,t\right)u\left(x_2,t\right) - \rho\left(x_1,t\right)u\left(x_1,t\right)\right] &= 0. \end{aligned} \tag{2.2}$$

If the boundaries x_1 and x_2 are moving with the fluid, i.e. if

$$\frac{dx_1}{dt} = u\left(x_1,t\right) \quad , \quad \frac{dx_2}{dt} = u\left(x_2,t\right), \tag{2.3}$$

then (2.2) simplifies to the classical integral form of the tracer conservation equation

$$\frac{dM\left(x_1,x_2,t\right)}{dt} \equiv \frac{d}{dt}\left(\int_{x_1(t)}^{x_2(t)} \rho\left(x,t\right)dx\right) = 0. \tag{2.4}$$

Eq. (2.4) simply states that the mass $M\left(x_1,x_2,t\right)$ contained between any two boundaries $x_1\left(t\right)$ and $x_2\left(t\right)$, moving with the fluid, is invariant in time, i.e. M is conserved.

Since $x_1\left(t\right)$ and $x_2\left(t\right)$ in (2.4) are any two points travelling with the fluid, one can consider (see Fig. 1) that these moving boundaries instantaneously coincide at time t^{n+1} with the boundaries of an Eulerian CV (ECV), whilst their upstream positions $x_1\left(t^n\right)$ and $x_2\left(t^n\right)$ at time t^n form the left and right boundaries of the associated upstream Lagrangian CV (LCV). In other words, the fluid contained in the Lagrangian segment $\left[x_1^d, x_2^d\right] \equiv \left[x_1\left(t^n\right), x_2\left(t^n\right)\right]$ is transported to the Eulerian segment $\left[x_1\left(t^{n+1}\right), x_2\left(t^{n+1}\right)\right]$, and this provides the basis of the SLICE-1D scheme.

To discretise (2.4), consider the general case where the computational 1D domain $\Omega = [x_{min}, x_{max}]$ is subdivided into N ECV's with unequal spacing $\Delta x_i \equiv x_{i+1/2} - x_{i-1/2}$ $(i = 1,2,..,N)$, where $x_{i-1/2}$ and $x_{i+1/2}$ are respectively the left and right boundaries of ECV_i. It is also convenient to define N associated grid points x_i at the centres of ECV's, i.e. $x_i \equiv \left(x_{i+1/2} + x_{i-1/2}\right)/2$, where the gridbox-averaged densities are placed. Defining the gridbox-averaged density at time t as

$$\overline{\rho}_i\left(t\right) \equiv \frac{1}{\Delta x_i}\int_{x_{i-1/2}}^{x_{i+1/2}} \rho\left(x,t\right)dx \equiv \frac{1}{\Delta x_i} M\left(x_{i-1/2}, x_{i+1/2}, t\right) \equiv \frac{M_i}{\Delta x_i}, \tag{2.5}$$

the time-discretisation of (2.4) can then be rewritten in a semi-Lagrangian fashion as

$$\overline{\rho}_i^{n+1} \equiv \overline{\rho}_i\left(t^{n+1}\right) \equiv \frac{\left(M_i\right)^{n+1}}{\Delta x_i} = \frac{\left(M_i^d\right)^n}{\Delta x_i}, \tag{2.6}$$

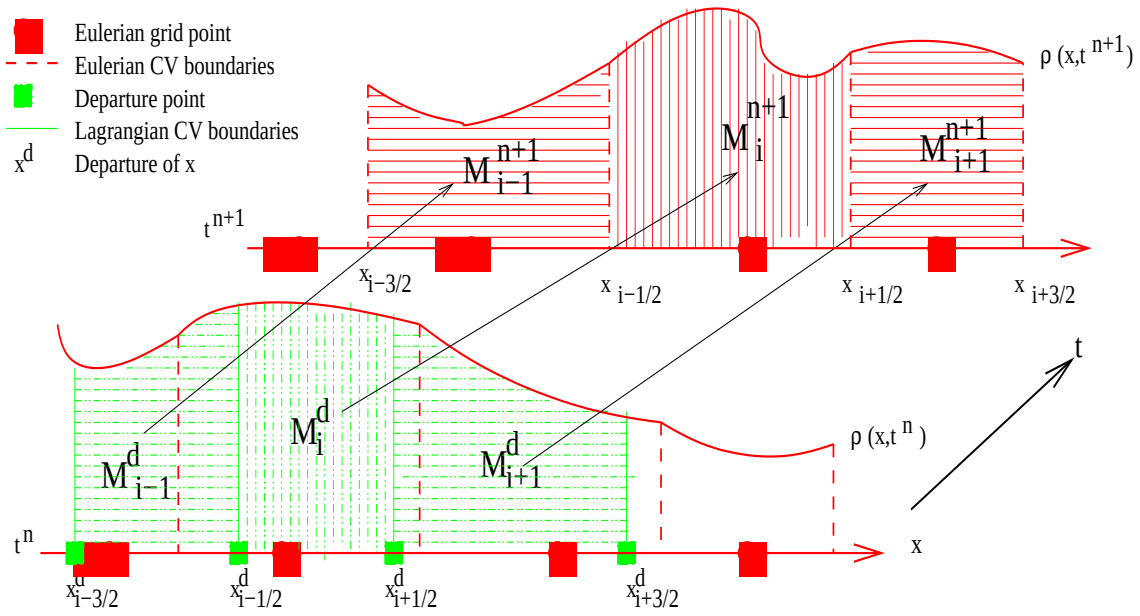

Figure 1: *Schematic for SLICE-1D. Given a gridbox-averaged density distribution* $\overline{\rho}(x_i, t^n)$ *and the departure points* $x^d_{i\pm1/2}$ *of an* ECV_i *at time* t^{n+1} *with boundaries at* $x = x_{i\pm1/2}$*, then* $\overline{\rho}(x_i, t^{n+1})$ *is computed from the transported mass* $(M_i)^{n+1} = (M_i^d)^n$*, where* $(M_i^d)^n$ *is the mass contained within the segment* $x \in \left[x^d_{i-1/2}, x^d_{i+1/2}\right]$ *at time* t^n*.*

where

$$M_i^d \equiv \int_{x^d_{i-1/2}}^{x^d_{i+1/2}} \rho(x,t)\, dx, \tag{2.7}$$

superscript n denotes evaluation at time t^n, superscript d denotes association with a departure-point value, and $x^d_{i-1/2}$ and $x^d_{i+1/2}$ are respectively the left- and right- hand boundaries of LCV_i at time t^n.

In general the shape of $\rho(x, t^n)$ is not known *a priori* and therefore a piecewise representation that uses the given discrete gridbox-averaged values is usually adopted. This can be either the Piecewise Constant Method (PCoM), Piecewise Linear Method (PLM) (van Leer 1977), Piecewise Parabolic Method (PPM) (Colella & Woodward (1984), Laprise & Plante (1995)) or the Piecewise Cubic Method (PCM) introduced herein. Since PCoM, PLM and PPM are all special (lower-order) cases of PCM, only PCM is described herein.

2.1 The Piecewise Cubic Method (PCM)

(a) Definition of the cubic

In a similar manner to the PPM, one can construct a density profile over the whole domain using a series of local cubics. For any ECV_i, defined over the segment $[x_{i-1/2}, x_{i+1/2}]$, a cubic polynomial for density distribution at time t^n can be uniquely defined (see solid curve of Fig. 2) as

$$\rho_i(\xi) = a_i^{(0)} + a_i^{(1)}\xi + a_i^{(2)}\xi^2 + a_i^{(3)}\xi^3 \quad , \quad \xi \in [0,1], \tag{2.8}$$

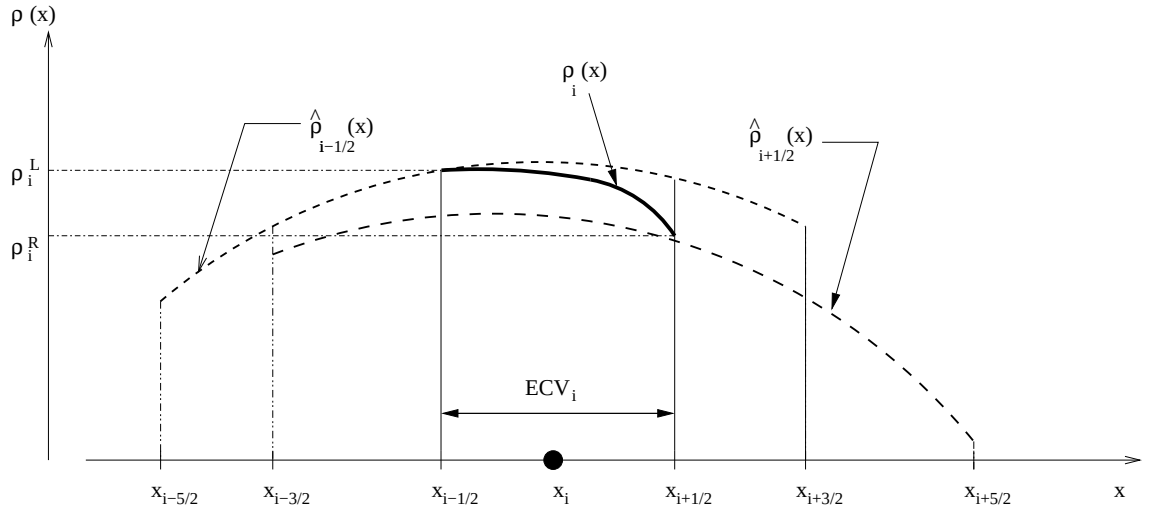

Figure 2: *Schematic for PCM.* $\rho_i(x)$ *(solid curve) is the piecewise-cubic representation of* $\rho(x)$ *for* ECV_i*, and* $\widehat{\rho}_{i\pm1/2}(x)$ *(dashed curves) are local cubics used to compute the associated parameters* ρ_i^L*,* ρ_i^R *and* $\delta\rho_i$*. The separation between curves is exaggerated for clarity and they consequently do not exactly satisfy* (2.14)-(2.16).

where $\xi = \left(x - x_{i-1/2}\right)/\Delta x_i$ is a dimensionless local variable, and $\left(a_i^{(0)}, a_i^{(1)}, a_i^{(2)}, a_i^{(3)}\right)$ are coefficients defined such that

$$\rho_i(0) = \rho_i^L, \tag{2.9}$$

$$\rho_i(1) = \rho_i^R, \tag{2.10}$$

$$\int_0^1 \rho_i(\xi)\, d\xi = \overline{\rho}_i, \tag{2.11}$$

$$\left.\frac{d\rho_i}{d\xi}\right|_{\xi=1/2} = \delta\rho_i. \tag{2.12}$$

Here ρ_i^L and ρ_i^R are respectively local estimates of ρ at the left- and right- hand edges of ECV_i, and $\delta\rho_i$ is a scaled slope $\Delta x_i \left(d\rho/dx\right)|_{x_i}$ of the density-distribution at its centre (see Section 2b for details of how this is done).

The solution to (2.9)-(2.12) yields

$$\left.\begin{aligned} a_i^{(0)} &= \rho_i^L, \\ a_i^{(1)} &= -6\rho_i^L + 6\overline{\rho}_i - 2\delta\rho_i, \\ a_i^{(2)} &= 9\rho_i^L - 3\rho_i^R - 6\overline{\rho}_i + 6\delta\rho_i, \\ a_i^{(3)} &= -4\rho_i^L + 4\rho_i^R - 4\delta\rho_i. \end{aligned}\right\} \tag{2.13}$$

(b) Computation of the cubic parameters ρ_i^L*,* ρ_i^R *and* $\delta\rho_i$

The density values at the edges of ECV_i, namely ρ_i^L and ρ_i^R, can be computed in a similar way to the PPM (Colella & Woodward 1984). This approach, of computing the edge values by differentiating a locally-defined *quartic cumulative mass* function, is formally equivalent to evaluating a *cubic density* function $\widehat{\rho}_{i-1/2}(x)$ at $x_{i-1/2}$, i.e.

$$\rho_i^L = \widehat{\rho}_{i-1/2}\left(x_{i-1/2}\right), \tag{2.14}$$

where (leftmost dashed curve of Fig. 2) the cubic density function $\widehat{\rho}_{i-1/2}(x)$ is centred about the point $x_{i-1/2}$. It is constructed to have specified masses $\Delta x_{i-2}\overline{\rho}_{i-2}$, $\Delta x_{i-1}\overline{\rho}_{i-1}$, $\Delta x_i\overline{\rho}_i$ and $\Delta x_{i+1}\overline{\rho}_{i+1}$ in the four immediately surrounding ECV's, i.e. to satisfy the four conditions

$$\left.\begin{array}{rcl} \int_{x_{i+1/2}}^{x_{i+3/2}} \widehat{\rho}_{i-1/2}(x)\,dx &=& \Delta x_{i+1}\overline{\rho}_{i+1}, \\ \int_{x_{i-1/2}}^{x_{i+1/2}} \widehat{\rho}_{i-1/2}(x)\,dx &=& \Delta x_i\overline{\rho}_i, \\ \int_{x_{i-3/2}}^{x_{i-1/2}} \widehat{\rho}_{i-1/2}(x)\,dx &=& \Delta x_{i-1}\overline{\rho}_{i-1}, \\ \int_{x_{i-5/2}}^{x_{i-3/2}} \widehat{\rho}_{i-1/2}(x)\,dx &=& \Delta x_{i-2}\overline{\rho}_{i-2}. \end{array}\right\} \tag{2.15}$$

To ensure continuity of $\rho(x)$ across CV boundaries, ρ_i^R is similarly obtained (see Fig. 2) from

$$\rho_i^R = \rho_{i+1}^L = \widehat{\rho}_{i+1/2}\left(x_{i+1/2}\right), \tag{2.16}$$

where $\widehat{\rho}_{i+1/2}(x)$ satisfies (2.15) but with the index shift $i \to i+1$.

The slope $(d\rho/dx)|_{x_i}$ at the centre of ECV_i is computed as the average of the two slopes $\left[d\widehat{\rho}_{i-1/2}(x)/dx\right]\big|_{x_i}$ and $\left[d\widehat{\rho}_{i+1/2}(x)/dx\right]\big|_{x_i}$. Thus the required scaled slope $\delta\rho_i$ is

$$\delta\rho_i = \frac{\Delta x_i}{2}\left[\left.\frac{d\widehat{\rho}_{i-1/2}(x)}{dx}\right|_{x_i} + \left.\frac{d\widehat{\rho}_{i+1/2}(x)}{dx}\right|_{x_i}\right]. \tag{2.17}$$

Computing the slopes in this way has the property that if $\rho(x)$ happens to be a globally-defined cubic then $\rho_i(x)$ coincides exactly with $\rho(x)$ over the interval $[x_{i-1/2}, x_{i+1/2}]$ and there is no error. This would not, for example, be the case if $(d\rho/dx)|_{x_i}$ were to be instead computed as the average of the two slopes $\left[d\widehat{\rho}_{i-1/2}(x)/dx\right]\big|_{x_{i-1/2}}$ and $\left[d\widehat{\rho}_{i+1/2}(x)/dx\right]\big|_{x_{i+1/2}}$.

(c) Computation of piecewise integrals

Having defined the cubics $\rho_i(x)$ for each ECV_i, the mass $\left(M_i^d\right)^n$ contained in LCV_i, which extends over the segment $[x_{i-1/2}^d, x_{i+1/2}^d]$ at time t^n, is computed as

$$\begin{aligned} \left(M_i^d\right)^n &= \int_{x_{i-1/2}^d}^{x_{i+1/2}^d} \rho(x,t^n)\,dx \\ &= \begin{cases} \Delta x_l \int_{\xi_{i-1/2}^d}^1 \rho_l^n(\xi)\,d\xi + \sum_{j=l+1}^{m-1} \Delta x_j \overline{\rho}_j^n + \Delta x_m \int_0^{\xi_{i+1/2}^d} \rho_m^n(\xi)\,d\xi, & m \geq l+1, \\ \Delta x_l \int_{\xi_{i-1/2}^d}^{\xi_{i+1/2}^d} \rho_l^n(\xi)\,d\xi, & m = l. \end{cases} \end{aligned} \tag{2.18}$$

Here l and $m \geq l$ are the ECV indices associated with the segments in which $x_{i-1/2}^d$ and $x_{i+1/2}^d$ lie, i.e. $x_{i-1/2}^d \in [x_{l-1/2}, x_{l+1/2}]$ and $x_{i+1/2}^d \in [x_{m-1/2}, x_{m+1/2}]$. Also $\xi_{i\pm1/2}^d$ are the local coordinates corresponding to $x_{i\pm1/2}^d$, i.e. $\xi_{i-1/2}^d = \left(x_{i-1/2}^d - x_{l-1/2}\right)/\Delta x_l$ and $\xi_{i+1/2}^d = \left(x_{i+1/2}^d - x_{m-1/2}\right)/\Delta x_m$. The integrals on the r.h.s. of (2.18) are evaluated analytically.

3 The SLICE-2D scheme

The nomenclature of Nair, Côté & Staniforth (1999*b*) is adopted herein whereby the arrival points at time t^{n+1} collectively define an Eulerian (x,y) mesh which subdivides the entire computational domain into a

finite number of contiguous and non-overlapping regular 2D ECV's, and similarly, the departure points at time t^n collectively define a Lagrangian (X, Y) mesh which subdivides the same domain into an equal number of contiguous and non-overlapping irregular 2D LCV's.

Consider a 2D domain $\Omega = [x_{min}, x_{max}] \times [y_{min}, y_{max}]$ subdivided into $N_x \times N_y$ ECV's with centres (x_i, y_j), $i = 1, .., N_x$, $j = 1, ..., N_y$, and whose boundaries are the straight lines that join the four corner points $\left(x_{i\pm1/2}, y_{j\pm1/2}\right)$, $i = 1, .., N_x$, $j = 1, ..., N_y$. The curvilinear Lagrangian coordinate system, which corresponds to the transformed Eulerian (x, y) system by the action of the velocity field over the time interval $\left[t^n, t^{n+1}\right]$, is denoted by (X, Y). A y_j-line of the Eulerian grid is the horizontal line defined by the set of points $\left\{\left(x_{i-1/2}, y_j\right),\ i = 1, .., N_x + 1\right\}$ and the Lagrangian Y_i is the curve defined by the set of points $\left\{\left(\widetilde{x}_{i,j-1/2}, \widetilde{y}_{i,j-1/2}\right),\ j = 1, .., N_y + 1\right\}$. These latter points are the centre points of the bottom edges of $LCV_{i,j}$ along the Lagrangian $X_{j-1/2}$, i.e. $\left(\widetilde{x}_{i,j-1/2}, \widetilde{y}_{i,j-1/2}\right) = \left[\left(x^d_{i-1/2}, y^d_{j-1/2}\right) + \left(x^d_{i+1/2}, y^d_{j-1/2}\right)\right]/2$, where $\left(x^d, y^d\right)$ denotes the departure point of (x, y). See details in Fig. 3.

The conservative scheme in 2D is a combination of the cascade approach and the SLICE-1D algorithm. It comprises a multiple sweep of SLICE-1D along one of the two Eulerian (Cartesian) directions followed by a similar multiple sweep along one of the two Lagrangian ones. Without *a priori* knowledge of the flow, there are no arguments for or against a particular choice of order in which directional sweeps are performed in Cartesian geometry, but for atmospheric flows in spherical geometry there can be (Nair, Côté & Staniforth 1999*a*). To facilitate possible generalisation of the present work to spherical geometry, the Nair et al. (1999*b*) choice of a first cascade along Eulerian x (holding y constant), followed by one along the Lagrangian Y (holding X constant), has been adopted. Cascading first along Eulerian y, then along Lagrangian X is however an equally valid choice for Cartesian geometry.

Consistent with the adopted CV approach, the problem considered here is the evaluation of the time evolution of the density averaged over an Eulerian gridbox, i.e. given $\overline{\rho}\,(x, y, t^n)$, compute $\overline{\rho}\,\left(x, y, t^{n+1}\right)$. This is distinct from the alternative gridpoint approach of evaluating the time evolution of the local, pointwise-defined, density $\rho\,(x, y, t)$. To achieve conservation, which is the cornerstone of the present scheme, the scheme advectively transports the quantity to be conserved (mass in this case), then computes the gridbox-averaged density at the new time step from the mass that arrives at the ECV at time t^{n+1}. This is equivalent to simply computing the elementary masses of LCV's, then translating them to their corresponding ECV's.

The first stage of the scheme is the computation of masses $ME_{i,j}$ contained in $ECV_{i,j}$, associated with Eulerian grid-points (x_i, y_j), then redistribution of them in a conservative way among $IECV_{i,j}$ (Intersection Eulerian Control Volumes) using the SLICE-1D algorithm described in the previous section. ($IECV$'s are intermediate CV's associated with surrounding intersection points and aligned along the first cascade direction x, see Fig. 3.) The second stage is to transfer the masses at $IECV_{i,j}$ to $ILCV_{i,j}$ (Intersection Lagrangian Control Volumes) and to then redistribute them conservatively to $LCV_{i,j}$ using the same SLICE-1D algorithm, again see Fig. 3. ($ILCV$'s are also intermediate CV's associated with surrounding intersection points but aligned along the second cascade direction Y.)

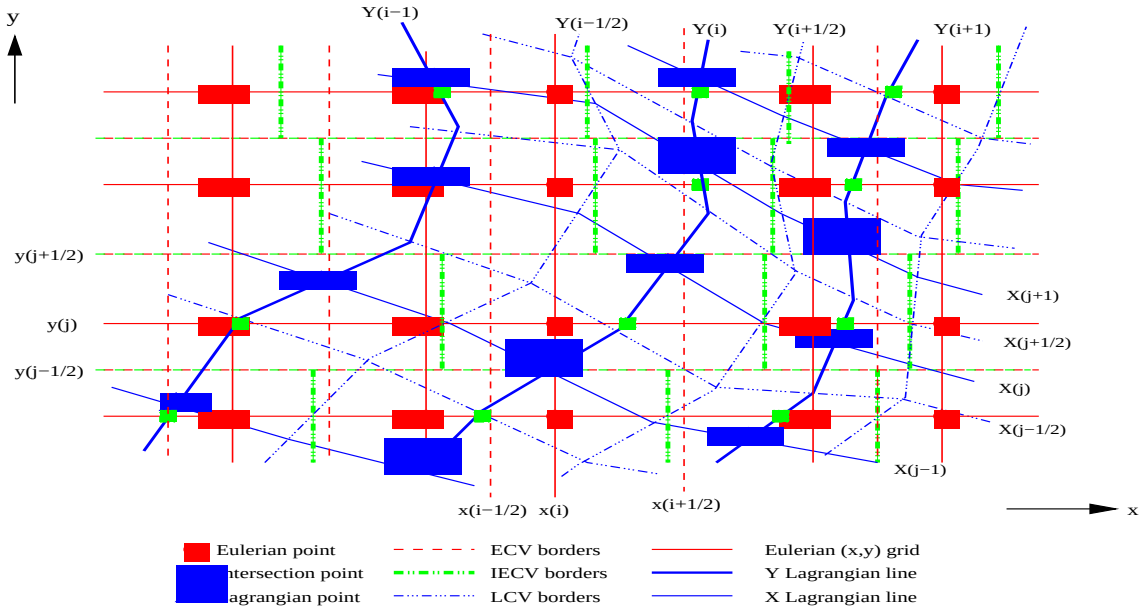

Figure 3: *Superposition of Eulerian* (x, y) *and Lagrangian* (X, Y) *coordinate systems and their associated grid-points and control-volumes.*

3.1 First stage

(a) computation of intersection points

As in Nair et al. (1999*b*), the Lagrangian grid (X_j, Y_i) is the linkage of Lagrangian points by straight lines in Eulerian space. Thus Y_i is linear (in $x - y$ coordinates) in the region of an intersection. The intersection points $\left(x'_{i-1/2,j}, y_j\right)$ between $Y_{i-1/2}$ and y_j are computed using linear interpolation as in Nair et al. (1999*b*), and similarly for the intersection points $\left(x'_{i,j}, y_j\right)$.

(b) Transfer of mass to intersection control volumes (IECV)

For simplicity and clarity, we denote by $ECV_{i,j}$ the Eulerian Control Volume surrounding the Eulerian grid-point (x_i, y_j) whose area is $EA_{i,j} = (x_{i+1/2} - x_{i-1/2}) \times (y_{j+1/2} - y_{j-1/2})$, whereas $IECV_{i,j}$ denotes the CV associated with the intersection point $\left(x'_{i,j}, y_j\right)$ whose area is $IEA_{i,j} = \left(x'_{i+1/2,j} - x'_{i-1/2,j}\right) \times (y_{j+1/2} - y_{j-1/2})$ (see Fig. 4). Since $ECV_{i,j}$ and $IECV_{i,j}$ share the same boundaries in the y-direction, $IECV_{i,j}$ has an inherently Eulerian flavour and therefore the name of Intersection-Eulerian CV seems appropriate. It is worth noting that for each column Y_i two intersection points are computed: (i) $\left(x'_{i-1/2,j}, y_j\right)$ which is the intersection between $Y_{i-1/2}$ and y_j and this gives directly the left boundary of $IECV_{i,j}$, and (ii) $\left(x'_{i,j}, y_j\right)$ which is the intersection between Y_i and y_j and this gives directly the centre of mass for $IECV_{i,j}$. Note also that the centre of mass for $IECV_{i,j}$ is not necessarily the geometric centre of $IECV_{i,j}$.

The first stage of the scheme is to redistribute conservatively the given masses from $ECV_{i,j}$ to $IECV_{i,j}$. This is done using SLICE-1D. To illustrate this process, let us consider a single y_j-strip of Fig. 3, shown in more detail in Fig. 4.

Given the masses

$$ME^n_{i,j} = \overline{\rho}^n_{i,j} \Delta x_i \Delta y_j, \tag{3.19}$$

of each $ECV_{i,j}$, an underlying cubic pseudo-density (or mass per unit length along the first cascade direction x) distribution for each $ECV_{i,j}$ can be defined as

$$\rho_{i,j}(\xi) = a^{(0)}_{i,j} + a^{(1)}_{i,j}\xi + a^{(2)}_{i,j}\xi^2 + a^{(3)}_{i,j}\xi^3 \quad , \quad \xi \in [0,1]. \tag{3.20}$$

In (3.20), $a^{(0)}_{i,j}$, $a^{(1)}_{i,j}$, $a^{(2)}_{i,j}$ and $a^{(3)}_{i,j}$ are defined (cf (2.9) - (2.12)) such that

$$\rho_{i,j}(0) = \rho^L_{i,j}, \tag{3.21}$$

$$\rho_{i,j}(1) = \rho^R_{i,j}, \tag{3.22}$$

$$\int_0^1 \rho_{i,j} d\xi = \frac{ME^n_{i,j}}{\Delta x_i}, \tag{3.23}$$

$$\left.\frac{d\rho_{i,j}}{d\xi}\right|_{\xi=1/2} = \delta\rho_{i,j}, \tag{3.24}$$

where, for fixed j, $\rho^L_{i,j}$, $\rho^R_{i,j}$ and $\delta\rho_{i,j}$ are computed using (2.14), (2.16) and (2.17), respectively. The mass $MI^n_{i,j}$ associated with each $IECV_{i,j}$ is then computed in a piecewise manner, using (2.18), as

$$MI^n_{i,j} = \begin{cases} \Delta x_l \int_{\xi'_{i-1/2,j}}^1 \rho_{l,j}(\xi)\, d\xi + \sum_{k=l+1}^{m-1} ME^n_{k,j} + \Delta x_m \int_0^{\xi'_{i+1/2,j}} \rho_{m,j}(\xi)\, d\xi, & m \geq l+1, \\ \Delta x_l \int_{\xi'_{i-1/2,j}}^{\xi'_{i+1/2,j}} \rho_{l,j}(\xi)\, d\xi, & m = l, \end{cases} \tag{3.25}$$

where $(l, m \geq l)$ are the ECV indices within which the boundaries of $IECV_{i,j}$ $\left(x'_{i-1/2,j}, x'_{i+1/2,j}\right)$ lie, and $\xi'_{i\pm1/2,j}$ are the points in local coordinates that correspond to $x'_{i\pm1/2,j}$. Noting that $l(i) \equiv m(i-1)$, and that by construction

$$\int_{x_{i-1/2}}^{x_{i+1/2}} \rho_{i,j} dx = ME^n_{i,j}, \tag{3.26}$$

it follows from (3.25) (with appropriate boundary conditions) that

$$\sum_{i=1}^{N_x} MI^n_{i,j} = \sum_{i=1}^{N_x} ME^n_{i,j}. \tag{3.27}$$

Here and throughout, it is assumed that all sets of CV's are contiguous and non-overlapping due to non-intersecting trajectories, i.e. the timestep Δt is chosen to satisfy the Lipschitz criterion (Smolarkiewicz & Pudykiewicz 1992) which also should ensure single valuedness of intersections $\left(x'_{i-1/2,j}, y_j\right)$ and $\left(x'_{i,j}, y_j\right)$ of the Lagrangian and Eulerian grids (Purser & Leslie 1991).

3.2 Second stage

The second stage consists of redistributing the masses $MI^n_{i,j}$ amongst the $LCV_{i,j}$ in a conservative way. Consider the curved Lagrangian strip around Y_i in Fig. 3, and shown in isolation in Fig. 5. Although in physical space (x, y) the $ILCV_{i,j}$'s and $LCV_{i,j}$'s are complex distorted areas, they are nevertheless regular in the Lagrangian space (X, Y), as illustrated in Fig. 6.

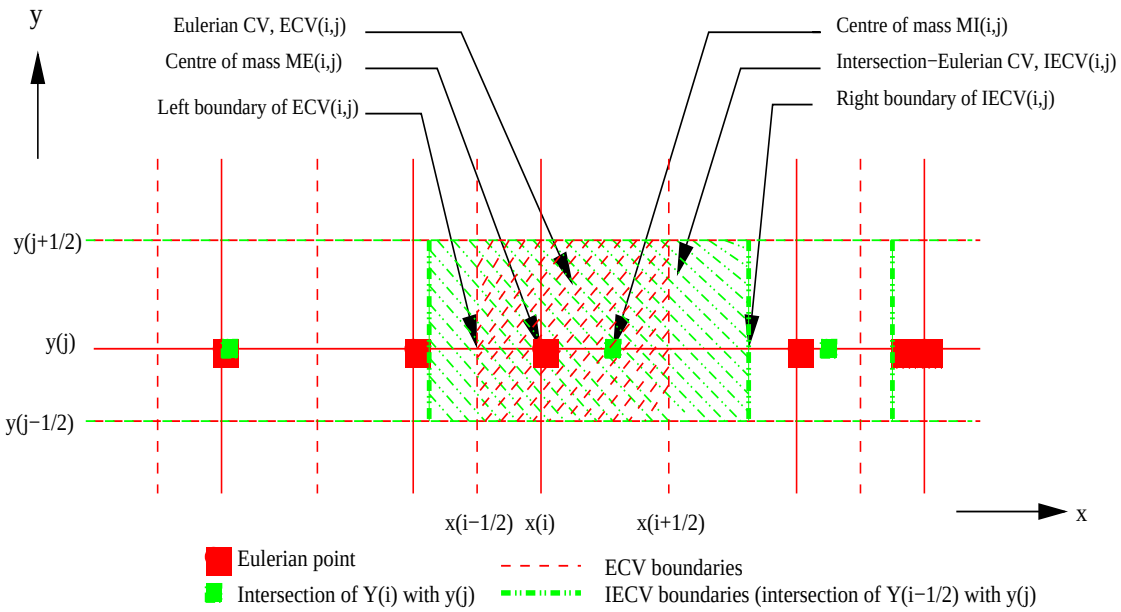

Figure 4: *First stage of SLICE-2D. The masses in $ECV_{i,j}$ are redistributed in a conservative manner to $IECV_{i,j}$.*

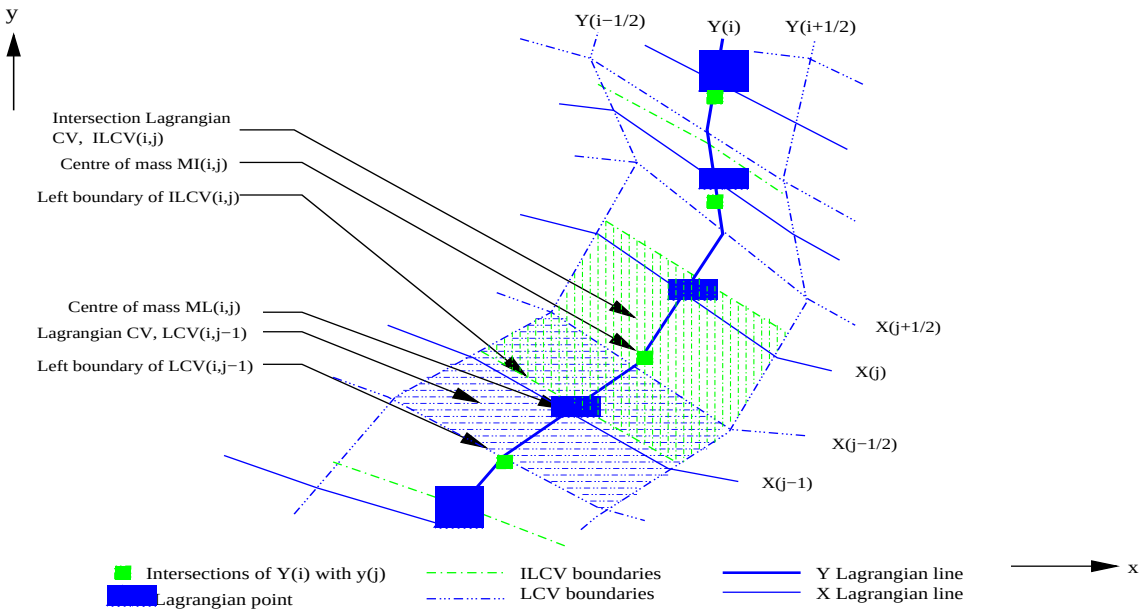

Figure 5: *Second stage of SLICE-2D. The masses in $IECV_{i,j}$ are transferred to $ILCV_{i,j}$ then redistributed in a conservative manner to $LCV_{i,j}$. $ILCV_{i,j}$ and $LCV_{i,j}$ are in physical space (x, y).*

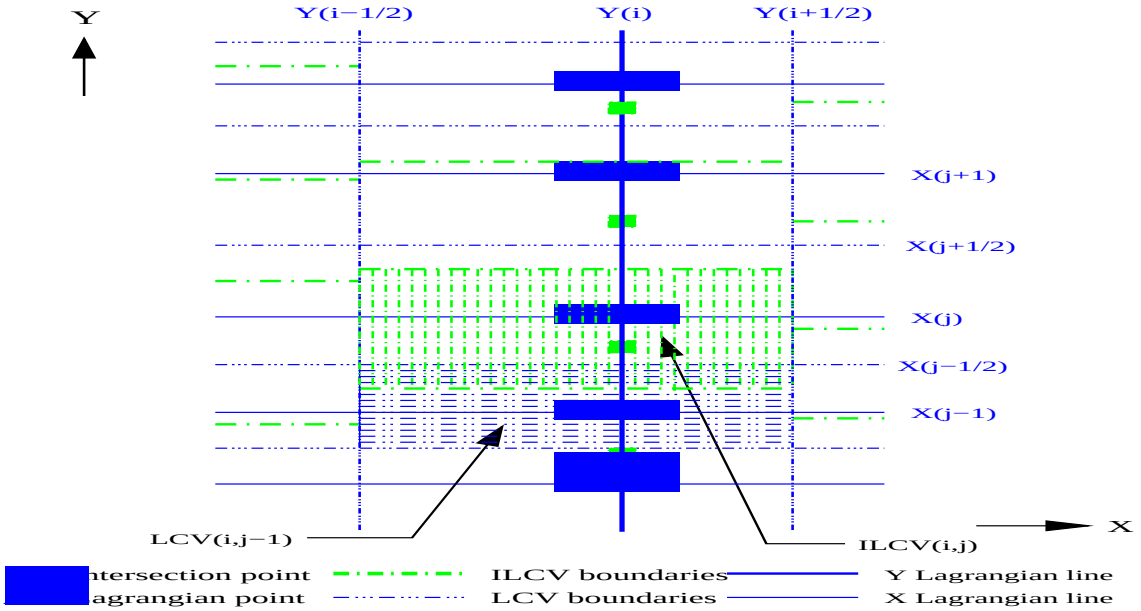

Figure 6: *Second stage of SLICE-2D. The masses in $ILCV_{i,j}$ are redistributed in a conservative manner to $LCV_{i,j}$. $ILCV_{i,j}$ and $LCV_{i,j}$ are depicted here in Lagrangian space (X,Y).*

First the masses associated with the $ILCV$'s need to be evaluated. This is done by making the approximation that each $ILCV$ actually has the same mass as its corresponding $IECV$. This is a reasonable approximation provided that the velocity field is smooth enough to give a sufficiently smooth distorted Lagrangian mesh. It is consistent with the assumption that the cascade approach is only accurate provided the velocity field has a sufficient degree of smoothness (Purser & Leslie 1991). The second stage of the remapping consists of one-dimensional integrations over $LCV_{i,j}$'s of local cubic pseudo-density functions $\widetilde{\rho}(s)$ (mass per unit length along the curved distance s of the Lagrangian Y_i). Similarly as the first stage, the $\widetilde{\rho}(s)$ are defined such that their integrals over $ILCV_{i,j}$'s have the associated masses $MI^n_{i,j}$ computed at the first stage. This requires specification of how $ILCV_{i,j}$'s and $LCV_{i,j}$'s overlap.

Recall that the Y_i curve is the set of elementary segments $s_{i,j-1/2}$ $(j = 1,..,N_y+1)$, linking the left boundaries $\left\{\left(\widetilde{x}_{i,j-1/2},\widetilde{y}_{i,j-1/2}\right),\ j=1,..,N_y+1\right\}$ of $LCV_{i,j}$'s, $j = 1,..,N_y$. From this the cumulative distance along Y_i from an arbitrary origin $\left(\widetilde{x}_{i,1/2},\widetilde{y}_{i,1/2}\right)$ to each point $\left(\widetilde{x}_{i,j-1/2},\widetilde{y}_{i,j-1/2}\right)$ is computed as

$$\begin{aligned} s_{i,1/2} &= 0, \\ s_{i,j+1/2} &= s_{i,j-1/2} + \sqrt{\left(\widetilde{x}_{i,j+1/2}-\widetilde{x}_{i,j-1/2}\right)^2 + \left(\widetilde{y}_{i,j+1/2}-\widetilde{y}_{i,j-1/2}\right)^2},\ j=1,..,N_y. \end{aligned} \tag{3.28}$$

Similarly $s'_{i,j}$ are the distances to the intersection points of Y_i with y_j, computed as

$$s'_{i,j} = s_{i,k-1/2} + \sqrt{\left(x'_{i,j}-\widetilde{x}_{i,k-1/2}\right)^2 + \left(y_j-\widetilde{y}_{i,k-1/2}\right)^2}, \tag{3.29}$$

where k is the CV index on the Y_i curve such that the intersection point $\left(x'_{i,j}, y_j > \widetilde{y}_{i,k-1/2}\right)$ belongs to the straight line that joins the two CV boundaries $\left(\widetilde{x}_{i,k-1/2},\widetilde{y}_{i,k-1/2}\right)$ and $\left(\widetilde{x}_{i,k+1/2},,\widetilde{y}_{i,k+1/2}\right)$. Two further pieces of information are required: (i) the locations of the centres of $LCV_{i,j}$ which are given simply by: $s_{i,j} = \left(s_{i,j+1/2}+s_{i,j-1/2}\right)/2$, and (ii) the boundaries of $LCV_{i,j}$ which are given by $s'_{i,j+1/2} = \left(s'_{i,j}+s'_{i,j+1}\right)/2$.

Having defined the topology, a cubic pseudo-density $\widetilde{\rho}(s)$ (or mass per unit length along the second cascade direction s, which defines the distance along the Lagrangian Y_i) can be fitted to the control volume $ILCV_{i,j}$, where $MI^n_{i,j}$ is known. An $ILCV_{i,j}$ associated cubic can be expressed in terms of a local non-dimensional variable $\zeta = \left(s - s'_{i,j-1/2}\right) / \left(s'_{i,j+1/2} - s'_{i,j-1/2}\right)$ as

$$\widetilde{\rho}_{i,j}(\zeta) = \widetilde{a}^{(0)}_{i,j} + \widetilde{a}^{(1)}_{i,j}\zeta + \widetilde{a}^{(2)}_{i,j}\zeta^2 + \widetilde{a}^{(3)}_{i,j}\zeta^3 \quad , \quad \zeta \in [0,1]. \tag{3.30}$$

In (3.30), $\widetilde{a}^{(0)}_{i,j}$, $\widetilde{a}^{(1)}_{i,j}$, $\widetilde{a}^{(2)}_{i,j}$ and $\widetilde{a}^{(3)}_{i,j}$ are coefficients such that

$$\widetilde{\rho}_{i,j}(0) = \widetilde{\rho}^L_{i,j}, \tag{3.31}$$

$$\widetilde{\rho}_{i,j}(1) = \widetilde{\rho}^R_{i,j}, \tag{3.32}$$

$$\int_0^1 \widetilde{\rho}_{i,j}(\zeta)\, d\zeta = \frac{MI^n_{i,j}}{\Delta s'_{i,j}}, \tag{3.33}$$

$$\left.\frac{d\widetilde{\rho}_{i,j}(\zeta)}{d\zeta}\right|_{\zeta=1/2} = \delta\widetilde{\rho}_{i,j}, \tag{3.34}$$

where $\Delta s'_{i,j} = s'_{i,j+1/2} - s'_{i,j-1/2}$. Here $\widetilde{\rho}^L_{i,j}$ and $\widetilde{\rho}^R_{i,j}$ are the pseudo-densities at the boundaries $\left(s'_{i,j-1/2}, s'_{i,j+1/2}\right)$, and $\delta\widetilde{\rho}_{i,j}$ denotes the scaled slope of pseudo-density profile at the centre of $ILCV_{i,j}$. These are computed in the same manner as previously detailed.

Once the cubics are defined for each $ILCV_{i,j}$, then the mass for each $LCV_{i,j}$ is computed in a similar manner to (3.25). Thus

$$ML^n_{i,j} = \begin{cases} \Delta s'_{i,k}\int_{\zeta_{i,j-1/2}}^{1} \widetilde{\rho}_{i,k}(\zeta)\, d\zeta + \sum_{l=k+1}^{p-1} MI^n_{i,l} + \Delta s'_{i,p}\int_0^{\zeta_{i,j+1/2}} \widetilde{\rho}_{i,p}(\zeta)\, d\zeta, & p \geq k+1, \\ \Delta s'_{i,k}\int_{\zeta_{i,j-1/2}}^{\zeta_{i,j+1/2}} \widetilde{\rho}_{i,k}(\zeta)\, d\zeta, & p = k, \end{cases} \tag{3.35}$$

where $(k, p \geq k)$ are the $ILCV$ indices where the boundaries $(s_{i,j-1/2}, s_{i,j+1/2})$ of $LCV_{i,j}$ lie, and $\zeta_{i,j\pm1/2}$ are the local coordinates corresponding to $s_{i,j\pm1/2}$. Again, noting that $k(j+1) \equiv p(j)$ and that by construction

$$\int_{s'_{i-1/2}}^{s'_{i+1/2}} \widetilde{\rho}_{i,j}\, dx = MI^n_{i,j}, \tag{3.36}$$

it follows from (3.35) (with appropriate boundary conditions) that

$$\sum_{j=1}^{N_y} ML^n_{i,j} = \sum_{j=1}^{N_y} MI^n_{i,j}, \tag{3.37}$$

provided that the $LCV_{i,j}$'s are contiguous and non-overlapping for reasons mentioned earlier.

Finally $\overline{\rho}^{n+1}_{i,j}$ is evaluated as

$$\overline{\rho}^{n+1}_{i,j} \equiv \frac{M^{n+1}_{i,j}}{\Delta x_i \Delta y_j} = \frac{\left(M^d_{i,j}\right)^n}{\Delta x_i \Delta y_j} = \frac{ML^n_{i,j}}{\Delta x_i \Delta y_j}. \tag{3.38}$$

The exact conservation property of the scheme then follows, using (3.19), (3.27) and (3.37), from

$$\begin{aligned} \sum_{i=1}^{N_x}\sum_{j=1}^{N_y} \overline{\rho}^{n+1}_{i,j}\Delta x_i \Delta y_j &= \sum_{i=1}^{N_x}\sum_{j=1}^{N_y} ML^n_{i,j} = \sum_{i=1}^{N_x}\left(\sum_{j=1}^{N_y} MI^n_{i,j}\right) = \sum_{j=1}^{N_y}\left(\sum_{i=1}^{N_x} MI^n_{i,j}\right) \\ &= \sum_{j=1}^{N_y}\sum_{i=1}^{N_x} ME^n_{i,j} = \sum_{i=1}^{N_x}\sum_{j=1}^{N_y} \overline{\rho}^n_{i,j}\Delta x_i \Delta y_j. \end{aligned} \tag{3.39}$$

The full algorithm can be summarised as:

SLICE-2D Algorithm

1. Define the corner points of $ECV_{i,j}$ to be $\left(x_{i\pm1/2}, y_{j\pm1/2}\right)$, $i = 1, .., N_x, j = 1, .., N_y$.
2. Given $\overline{\rho}^n_{i,j} \equiv \overline{\rho}\left(x_i, y_j, t^n\right)$, compute the mass $ME^n_{i,j} = \overline{\rho}^n_{i,j} EA_{i,j}$ of $ECV_{i,j}$.
3. Compute the cubic coefficients $\left(a^{(0)}_{i,j}, a^{(1)}_{i,j}, a^{(2)}_{i,j}, a^{(3)}_{i,j}\right)$ for each $ECV_{i,j}$.
4. Locate the corners of $LCV_{i,j}$ - these are the departure points for the corners of $ECV_{i,j}$, i.e. $\left(x^d_{i\pm1/2}, y^d_{j\pm1/2}\right)$.
5. Locate intersection points $\left(x'_{i,j}, y_j\right)$, see text for details.
6. Locate the $IECV_{i,j}$ boundaries $\left[x'_{i-1/2,j}, x'_{i+1/2,j}\right]$.
7. Compute the mass $MI^n_{i,j}$ of each $IECV_{i,j}$ using SLICE-1D.
8. Set the mass of each $ILCV_{i,j}$ equal to $MI^n_{i,j}$.
9. Compute the distances $s_{i,j}$ that define the boundaries of $LCV_{i,j}$ along Y_i.
10. Compute the distances $s'_{i,j}$ that define the boundaries of $ILCV_{i,j}$ along Y_i.
11. Compute the cubic coefficients $\left(\widetilde{a}^{(0)}_{i,j}, \widetilde{a}^{(1)}_{i,j}, \widetilde{a}^{(2)}_{i,j}, \widetilde{a}^{(3)}_{i,j}\right)$ for each $ILCV_{i,j}$.
12. Compute the mass $ML^n_{i,j}$ of each $LCV_{i,j}$ using SLICE-1D.
13. Transport $ML^n_{i,j}$ to its corresponding $ECV_{i,j}$ and compute $\overline{\rho}^{n+1}_{i,j} = ML^n_{i,j}/EA_{i,j}$.

3.3 Computational efficiency

For a problem in d dimensions, the cost of SLICE with a k^{th}-order polynomial piecewise representation increases only linearly with k and with d (i.e. it is $O\left(kd\right)$), whereas it is $O\left(k^d\right)$ for a standard Semi-Lagrangian (SL) scheme. SLICE has an additional overhead associated with the computation of intersections and piecewise cubic coefficients. No attempt has been made to optimise the present algorithm at this stage of development. However, preliminary CPU times for the 2D problems in Section 4 with $k = 3$ are relatively comparable to those of a standard SL scheme. Greater savings could be expected for 3D problems and higher-order polynomial remappings. Therefore the scheme is at least as efficient as current *a posteriori* conserving schemes.

4 Numerical examples

Three test problems from the literature (see e.g. Rancic (1995), Nair et al. (1999*b*), Pudykiewicz & Staniforth (1984), Sun & Yeh (1997)) are used to validate the proposed scheme and to compare its performance against that of a standard semi-Lagrangian scheme using bi-cubic interpolation. Note that the departure points for all the tests are computed analytically. This allows the comparison between pure classical interpolation (in the

context of semi-Lagrangian schemes) and the present conservative remappping, without the contamination of departure point error. However, for general problems, the departure points could be computed as in classical semi-Lagrangian schemes using the discrete velocity field (Staniforth & Côté 1991). For the tests described in this section, the two methods give virtually indistinguishable results and only those using exact trajectories are presented in what follows.

4.1 Definition of the idealised cyclogenesis problem

The idealised cyclogenesis problem (see e.g. Rancic (1995), Sun & Yeh (1997), Nair et al. (1999*b*)) consists of an initial circular vortex with a tangential velocity $V(r) = v_0 \tanh(r) / \cosh^2(r)$, where r is the radial distance from the centre of the vortex (x_c, y_c), and v_0 is a constant chosen such that the maximum value of $V(r)$ is unity (i.e. $V_{max} = 1$). The analytical solution $\rho(x, y, t)$ is

$$\rho(x, y, t) = -\tanh\left[\left(\frac{y - y_c}{\delta}\right)\cos(\omega t) - \left(\frac{x - x_c}{\delta}\right)\sin(\omega t)\right], \tag{4.40}$$

where $\omega = V(r)/r$ is the angular velocity and δ is constant.

4.2 Definition of the slotted cylinder problem

The slotted-cylinder problem (see e.g. Zalesak (1979), Sun & Yeh (1997), Nair et al. (1999*b*)) consists of solid-body rotation of a slotted cylinder in a flow field that rotates with constant angular velocity ω about a point (x_c, y_c). The analytical solution for $\rho(x, y, t)$ is

$$\rho(x, y, t) = \begin{cases} \rho_0 & \text{for } |\xi| \geq s_w/2,\ r \leq \sigma, \\ \rho_0 & \text{for } \zeta \geq s_l - \sigma,\ r \leq \sigma, \\ 0 & \text{otherwise,} \end{cases} \tag{4.41}$$

where ρ_0 is a constant, σ is the radius of the cylinder, s_w, s_l are the width and length of the slot respectively. Here r, ξ and ζ are defined with respect to the moving centre of the cylinder, i.e.

$$\begin{cases} \xi = x - x_c + \gamma\cos(\omega t), \\ \zeta = y - y_c + \gamma\sin(\omega t), \\ r = \left(\xi^2 + \zeta^2\right)^{1/2}, \end{cases} \tag{4.42}$$

where γ is the distance from the centre of the flow (x_c, y_c) to the centre of the cylinder $(x_c - \gamma\cos(\omega t), y_c - \gamma\sin(\omega t))$.

4.3 Definition of the cosine hill problem

This problem (see e.g. Pudykiewicz & Staniforth (1984)) is similar to the slotted cylinder one, except that the distribution is much smoother in space. The analytical solution $\rho(x, y, t)$ is

$$\rho(x, y, t) = \begin{cases} \rho_0\left[1 + \cos\left(\frac{\pi r}{\sigma}\right)\right]/2 & \text{for } r \leq \sigma, \\ 0 & \text{otherwise,} \end{cases} \tag{4.43}$$

where ρ_0, σ and r have the same definitions as for the slotted cylinder problem.

4.4 Results

For all the test problems, the initial state $\rho_0(x,y)$ is the analytical solution at $t=0$, i.e. $\rho_0(x,y)=\rho(x,y,0)$, and the analytical solution for the average density,

$$\overline{\rho}(x_i,y_j,t)=\left(\frac{1}{\Delta x_i \Delta y_j}\right)\int_{x_{i-1/2}}^{x_{i+1/2}}\int_{y_{j-1/2}}^{y_{j+1/2}}\rho(x,y,t)\,dxdy, \tag{4.44}$$

is computed, for convenience, using standard highly-accurate 10-point Gauss-Legendre quadrature (Press, Teukolsky, Vetterling & Flannery 1992).

Since SLICE-2D computes the evolution of gridbox-averaged density $\overline{\rho}(x_i,y_j,t)$, whereas standard semi-Lagrangian schemes compute pointwise density $\rho(x_i,y_j,t)$, two error measures are defined. These are:

$$rms_1=\left[\frac{1}{N_xN_y}\sum_{i=1}^{N_x}\sum_{j=1}^{N_y}\left(\rho_{i,j}^{an}-\rho_{i,j}^{num}\right)^2\right]^{1/2}, \tag{4.45}$$

the root-mean-square difference between the *pointwise* analytical solution $\rho^{an}(x_i,y_j,t)$ and the numerical one $\rho^{num}(x_i,y_j,t)$; and

$$rms_2=\left[\frac{1}{N_xN_y}\sum_{i=1}^{N_x}\sum_{j=1}^{N_y}\left(\overline{\rho}_{i,j}^{an}-\overline{\rho}_{i,j}^{num}\right)^2\right]^{1/2}, \tag{4.46}$$

the root-mean-square difference between the *gridbox-averaged* analytical solution $\overline{\rho}^{an}(x_i,y_j,t)$ and the numerical one $\overline{\rho}^{num}(x_i,y_j,t)$. On the one hand, the first measure, rms_1, is the natural measure for a standard (interpolating) SL method. For the comparisons described below, however, in calculating rms_1 for SLICE-2D, the gridbox-averaged numerical solution is used to approximate the pointwise numerical solution (i.e. $\left(\rho_{i,j}^{num}\right)\big|_{SLICE-2D}\approx\left(\overline{\rho}_{i,j}^{num}\right)\big|_{SLICE-2D}$ is assumed), and this arguably disadvantages the SLICE-2D method since rms_1 is not a natural error measure for it. On the other hand, the second measure, rms_2 is the natural error measure for the SLICE-2D solution, but not for a standard (interpolating) SL method so it is not presented for this latter method.

To measure the extent to which mass conservation is respected, a percentage deviation of the total mass from its initial value is defined as

$$pdm=100\times\left(M_T^n-M_T^0\right)/M_T^0, \tag{4.47}$$

where M_T^n is the total mass at timestep n given by

$$M_T^n=\sum_{i=1}^{N_x}\sum_{j=1}^{N_y}M\,E_{i,j}^n. \tag{4.48}$$

In addition to results using the SLICE-2D scheme described here, which employs a piecewise cubic representation, results using two further schemes are also presented. These schemes are identical in every respect to SLICE-2D except that "PPM1" uses the piecewise parabolic representation of Colella & Woodward (1984), whereas "PPM2" uses the piecewise parabolic representation of Laprise & Plante (1995).

Results for the three test problems are displayed in Tables 1 - 3 and Figs. 7 - 9.

It can be seen from Tables 1- 3 that, overall, in addition to achieving (to within machine precision) exact conservation, SLICE-2D is more accurate than the standard bicubic semi-Lagrangian scheme. This is most

Table 1: Cyclogenesis problem: $\Omega = [0, 10]^2$, uniform grid with $N_x = N_y = 129$, number of time steps $N_t = 16$, time step $\Delta t = 0.3125$, Courant number $C = V_{max}\Delta t / \min(\Delta x, \Delta y) = 4$.

	rms_1	rms_2	pdm [%]
Bicubic SL	0.074217	-	+0.2165E-14
SLICE(PPM1)	0.070100	0.031728	+0.4071E-14
SLICE(PPM2)	0.078770	0.040950	−0.5689E-14
SLICE(PCM)	0.069347	0.031070	+0.7275E-14

Table 2: Slotted cylinder problem: $\Omega = [0, 100]^2$, $\omega = 0.3635 \times 10^{-4} s^{-1}$, $N_x = N_y = 101$, $N_t = 576$ (6 rotations), $\Delta t \simeq 1800s$, $C \simeq 3.27$, $\rho_0 = 1$, $\gamma = 25$, $\sigma = 15$, $s_w = 6$, $s_l = 25$.

	rms_1	rms_2	pdm [%]
Bicubic SL	0.086937	-	−0.7310E-01
SLICE(PPM1)	0.070106	0.047171	−0.7746E-12
SLICE(PPM2)	0.087648	0.068697	−0.2039E-12
SLICE(PCM)	0.067331	0.043950	−0.7339E-12

Table 3: Cosine-hill problem: $\Omega = \left[0, 32 \times 10^5 m\right]^2$, $\omega = 10^{-5} s^{-1}$, $N_x = N_y = 33$, $N_t = 142$ (2 rotations), $\Delta t \simeq 8849.56s$, $C \simeq 2$, $\rho_0 = 100$, $\gamma = 8 \times 10^5 m$, $\sigma = 4 \times 10^5 m$.

	rms_1	rms_2	pdm [%]
Bicubic SL	3.844609	-	+0.7262E-00
SLICE(PPM1)	1.947452	1.745551	−0.1307E-13
SLICE(PPM2)	3.903246	3.691555	+0.7840E-12
SLICE(PCM)	1.597706	1.405720	+0.1437E-12

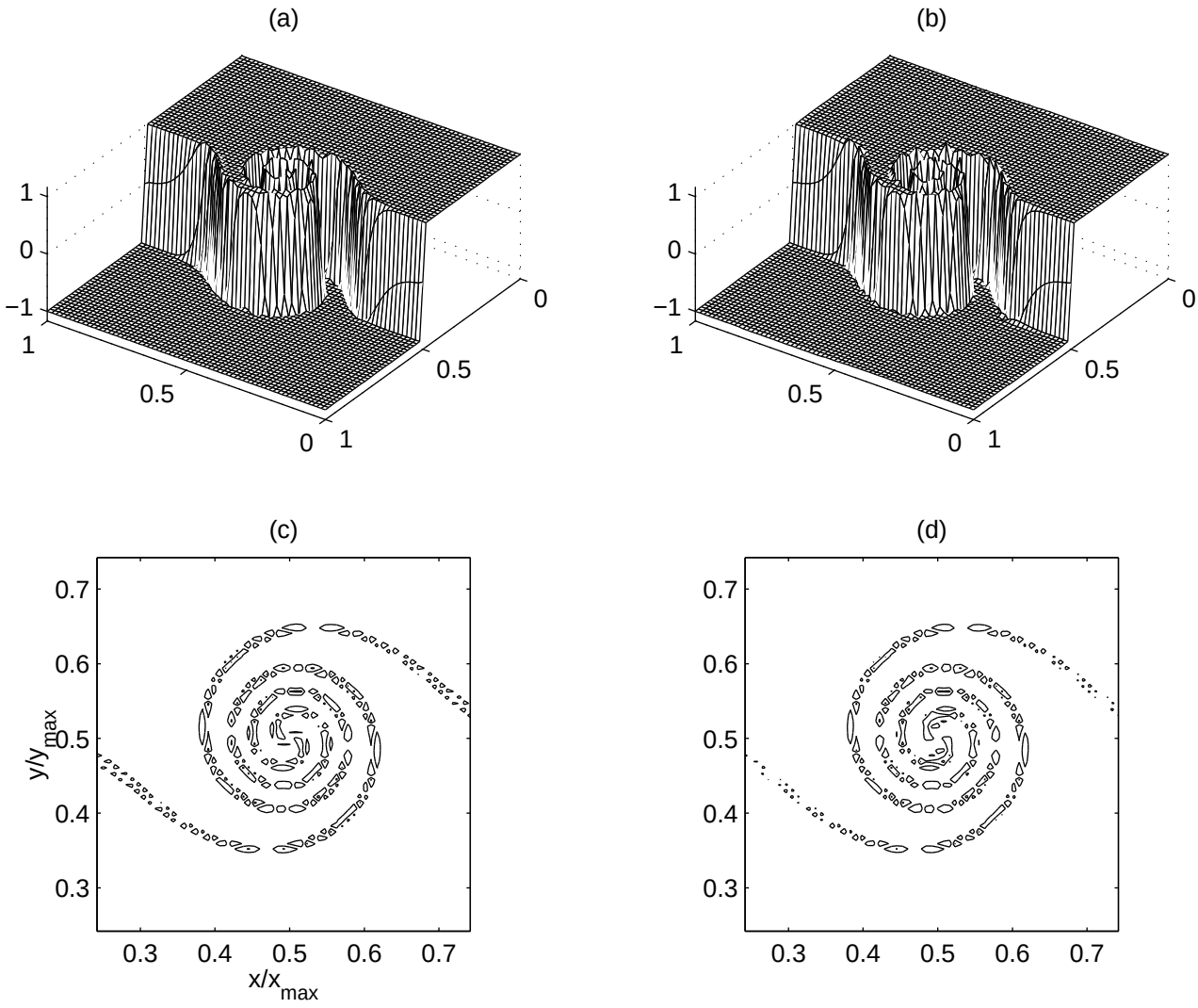

Figure 7: Cyclogenesis problem with parameters as in Table 1: (a) bicubic SL solution; (b) SLICE-2D (PCM) solution; (c) error (analytic minus numeric) for bicubic SL; (d) error for SLICE-2D(PCM). For (a) & (b), only every 2nd point in each direction is shown for pictorial clarity. For (c) & (d), contour min $\equiv Cont_{min} = -0.627$, contour interval $\equiv I_{cont} = 0.418$.

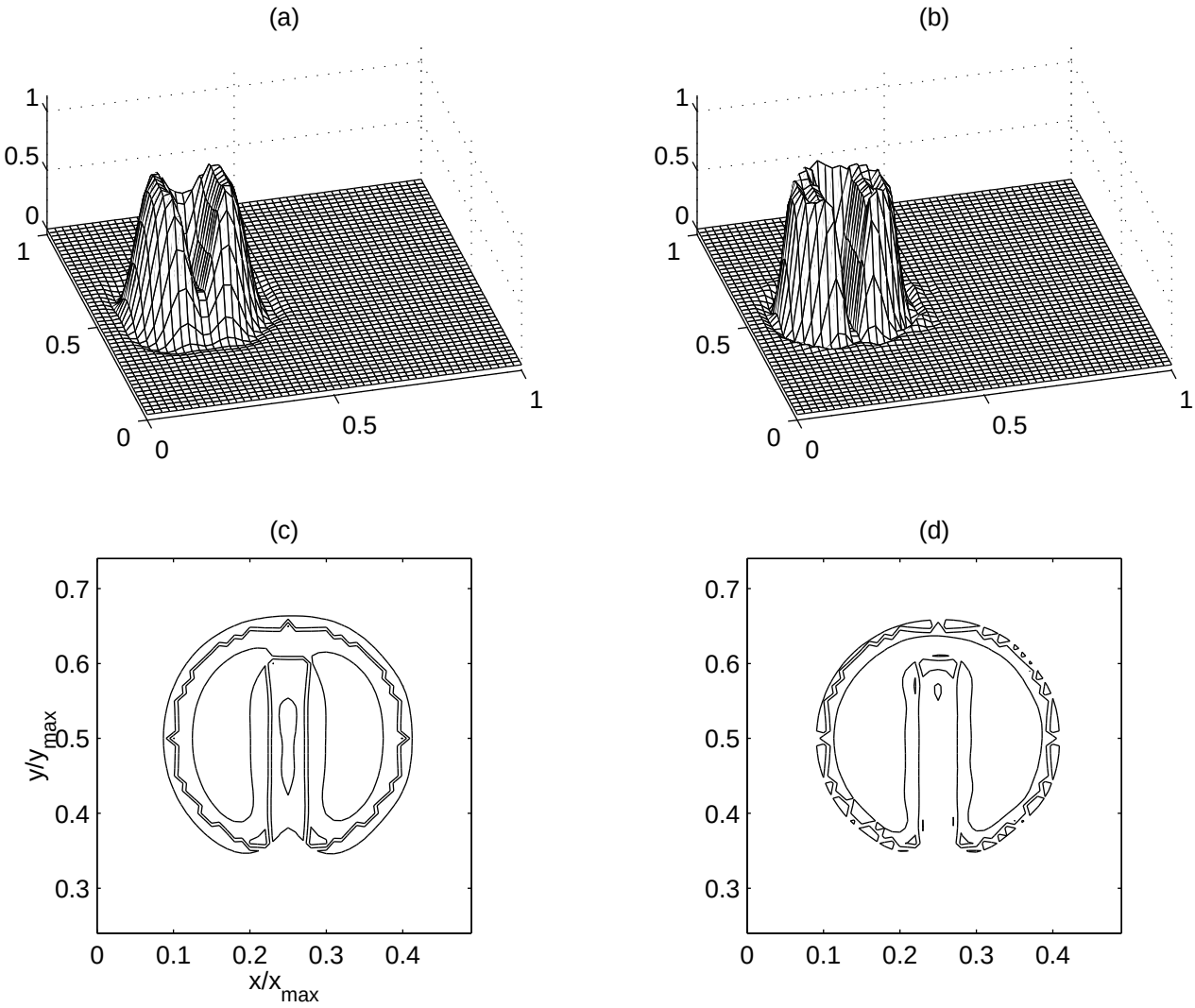

Figure 8: As in Fig. 7, but for the slotted-cylinder problem with parameters as in Table 2. For (a) & (b) only every 2nd point in each direction is shown for pictorial clarity. For (c) & (d), $Cont_{min} = -0.5266$, $I_{cont} = 0.3803$.

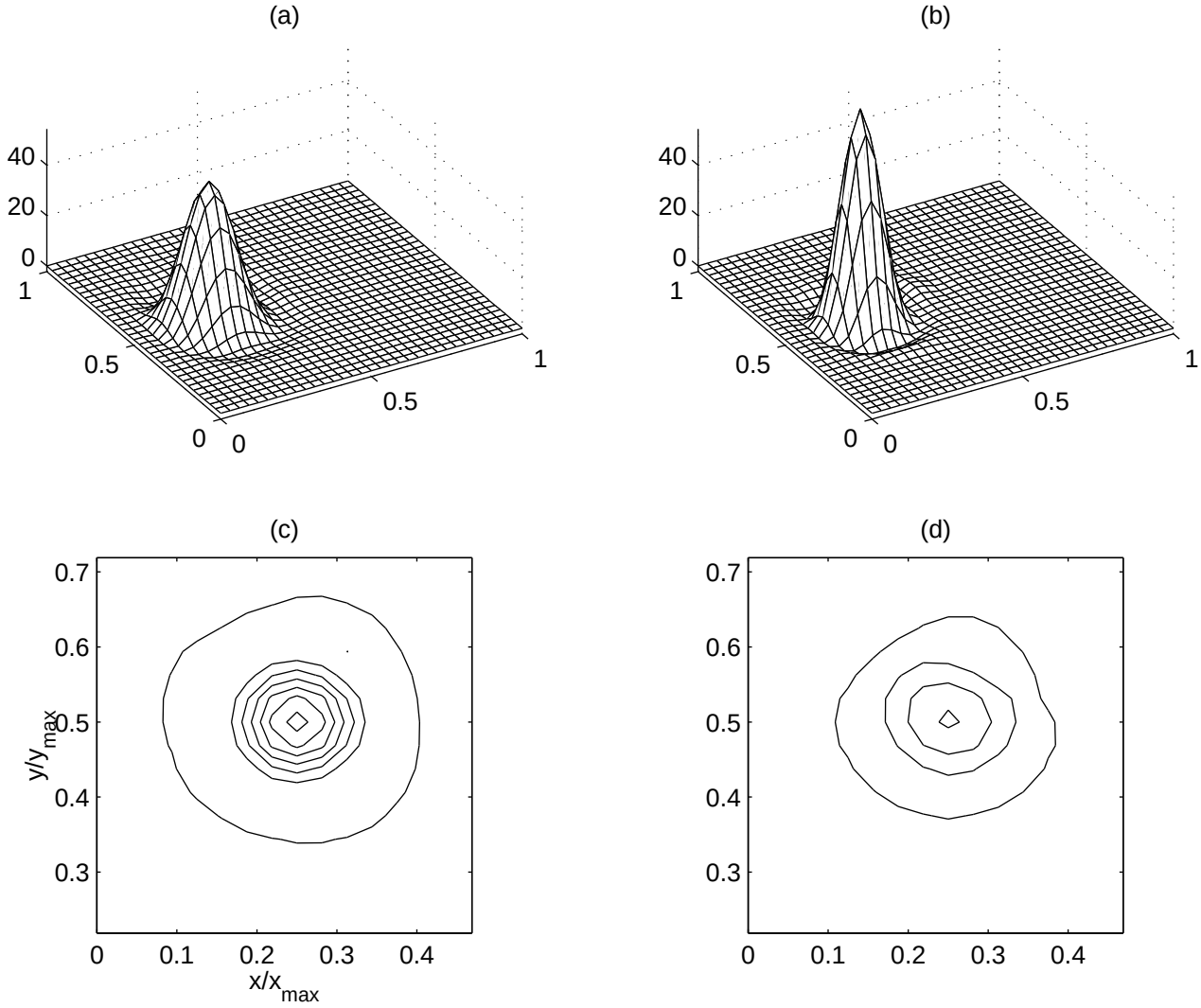

Figure 9: As in Fig. 7, but for the cosine-hill problem with parameters as in Table 3. For (a) & (b), all points shown. For (c), $Cont_{min} = -41.27$, $I_{cont} = 8.66$; and for (d), $Cont_{min} = -15.29$, $I_{cont} = 8.66$.

apparent with problem (c) where the distribution is smooth. If a piecewise parabolic representation is adopted instead of a piecewise cubic one, then the parabola advocated by Colella & Woodward (1984) (PPM1) is more accurate than that defined by Laprise & Plante (1995) (PPM2). This is probably because PPM1 is continuous across CV boundaries whereas PPM2 is not. It can also be seen that the mass conservation for the standard SL scheme is somewhat problematic and depends upon the length of integration. For example, it is almost exact for problem (a), although this is not due to a conservative attribute of the scheme but rather due to the anti-symmetry of the distribution, whereas it has generated a 0.7% mass increase from its initial value for the integration of problem (c). However, mass in SLICE-2D is exactly conserved irrespective of the piecewise representation, the length of integration, or the irregularity of the grid. Examination of Fig. 8 shows that the SLICE-2D(PCM) algorithm much better represents the slot than does the standard bicubic SL one. Similarly from Fig. 9, SLICE-2D(PCM) gives a sharper less-damped representation of the cosine hill.

5 Conclusions

A computationally efficient and inherently conservative semi-Lagrangian scheme for transport problems has been developed. Numerical tests show that the proposed scheme achieves competitive or better accuracy than that of standard non-conservative interpolating semi-Lagrangian schemes, and with a competitive computational cost. SLICE is also free of the usual complexity and the potential cost for implementation in full atmospheric models generally associated with conservative SL schemes. As for standard 3D cascade interpolation, the extension of the scheme from 2D to 3D Cartesian geometry appears to be relatively straightforward. In principle monotonocity can be included in an analogous manner as for PPM (Colella & Woodward 1984). However, unlike PPM, for PCM such an approach would involve a selection process for the right solution of a quadratic equation, which may prove costly. However, the alternative approach of using a general monotonicity filter, e.g. (Nair et al. 1999*b*), also appears viable and might be more efficient. Extension of the scheme to spherical geometry, on a latitude-longitude grid, will need careful consideration near the poles and the degree of complexity may depend on how the control volumes associated with the poles are defined.

References

Colella, P. & Woodward, P. 1984 , The piecewise parabolic method (PPM) for gas-dynamical simulations, *J. Comput. Phys.* **54**, 174–201.

Laprise, J. & Plante, A. 1995 , A class of semi-Lagrangian integrated mass (SLIM) numerical transport algorithms, *Mon. Wea. Rev.* **123**, 553–565.

Leslie, L. M. & Purser, R. J. 1995 , Three-dimensional mass-conserving semi-Lagrangian scheme employing forward trajectories, *Mon. Wea. Rev.* **123**, 2551–2566.

Machenhauer, B. & Olk, M. 1996 , On the development of a cell-integrated semi-Lagrangian shallow water model on the sphere, *in* 'ECMWF Workshop Proceedings: Semi-Lagrangian Methods', ECMWF, Reading, pp. 213–228.

Machenhauer, B. & Olk, M. 1997 , The implementation of the semi-implicit cell-integrated semi-Lagrangian models, *Atmos. Ocean (special issue)* **35**, 103–126.

Nair, R. & Machenhauer, B. 2002 , The mass conservative cell-integrated semi-Lagrangian advection scheme on the sphere, *Mon. Wea. Rev.* **130**, 649–667.

Nair, R., Côté, J. & Staniforth, A. 1999*a* , Cascade interpolation for semi-Lagrangian advection over the sphere, *Q. J. R. Meteorol. Soc.* **125**, 1445–1468.

Nair, R., Côté, J. & Staniforth, A. 1999*b* , Monotonic cascade interpolation for semi-Lagrangian advection, *Q. J. R. Meteorol. Soc.* **125**, 197–212.

Nair, R., Scroggs, J. & Semazzi, F. 2002 , Efficient conservative global transport schemes for climate and atmospheric chemistry models, *Mon. Wea. Rev.* (submitted).

Press, W., Teukolsky, S., Vetterling, W. & Flannery, B. 1992 , Numerical recipes in Fortran 77, Cambridge University Press, Cambridge UK.

Priestley, A. 1993 , A quasi-conservative version of the semi-Lagrangian advection scheme, *Mon. Wea. Rev.* **121**, 621–629.

Pudykiewicz, J. & Staniforth, A. 1984 , Some properties and comparative performance of the semi-Lagrangian method of Robert in the solution of the advection-diffusion equation, *Atmos.-Ocean* **22**, 283–308.

Purser, J. 1998 , Efficient high-order semi-Lagrangian methods, *in* 'ECMWF Workshop Proceedings: Recent developments in numerical methods for atmospheric modelling', ECMWF, Reading, pp. 73–94.

Purser, J. & Leslie, L. M. 1991 , An interpolation procedure for high-order three- dimensional semi-Lagrangian models, *Mon. Wea. Rev.* **119**, 2492–2498.

Rancic, M. 1992 , Semi-Lagrangian piecewise biparabolic scheme for two dimensional horizontal advection of passive scalar, *Mon. Wea. Rev.* **120**, 1394–1406.

Rancic, M. 1995 , An efficient conservative monotonic remapping for semi-Lagrangian transport algorithms, *Mon. Wea. Rev.* **123**, 1213–1217.

Scroggs, J. S. & Semazzi, F. H. M. 1995 , A conservative semi-Lagrangian method for multidimensional fluid dynamics applications, *Num. Meth. for PDEs* **11**, 445–452.

Smolarkiewicz, P. K. & Pudykiewicz, J. A. 1992 , A class of semi-Lagrangian approximations for fluids, *J. Atmos. Sci.* **49**, 2082–2096.

Staniforth, A. & Côté, J. 1991 , Semi-Lagrangian integration schemes for atmospheric models - a review, *Mon. Wea. Rev.* **119**, 2206–2223.

Sun, W. Y. & Yeh, K. S. 1997 , A general semi-Lagrangian advection scheme employing forward trajectories, *Q. J. R. Meteorol. Soc.* **123**, 2463–2476.

Temperton, C., Hortal, M. & Simmons, A. 2001 , A two-time-level semi-Lagrangian global spectral model, *Q. J. R. Meteorol. Soc.* **127**, 111–127.

van Leer, B. 1977 , Towards the ultimate conservative difference scheme IV: A new approach to numerical convection, *J. Comput. Phys.* **23**, 276–299.

Zalesak, S. T. 1979 , Fully multidimensional flux-corrected transport algorithms for fluids, *J. Comput. Phys.* **31**, 335–362.